Wind and Structures, *Vol. 29, No. 6 (2019) 389-403*
DOI: https://doi.org/10.12989/was.2019.29.6.389

Dimension-reduction simulation of stochastic wind velocity fields by two continuous approaches

Zhangjun Liu[1a], Chenggao He[2b], Zenghui Liu[1c] and Hailin Lu[*1]

[1]*School of Civil Engineering and Architecture, Wuhan Institute of Technology, Wuhan 430074, P.R. China*
[2]*College of Civil Engineering & Architecture, China Three Gorges University, Yichang 443002, P.R. China*

(Received January 22, 2019, Revised June 5, 2019, Accepted June 25, 2019)

Abstract. In this study, two original spectral representations of stationary stochastic fields, say the continuous proper orthogonal decomposition (CPOD) and the frequency-wavenumber spectral representation (FWSR), are derived from the Fourier-Stieltjes integral at first. Meanwhile, the relations between the above two representations are discussed detailedly. However, the most widely used conventional Monte Carlo schemes associated with the two representations still leave two difficulties unsolved, say the high dimension of random variables and the incompleteness of probability with respect to the generated sample functions of the stochastic fields. In view of this, a dimension-reduction model involving merely one elementary random variable with the representative points set owing assigned probabilities is proposed, realizing the refined description of probability characteristics for the stochastic fields by generating just several hundred representative samples with assigned probabilities. In addition, for the purpose of overcoming the defects of simulation efficiency and accuracy in the FWSR, an improved scheme of non-uniform wavenumber intervals is suggested. Finally, the Fast Fourier Transform (FFT) algorithm is adopted to further enhance the simulation efficiency of the horizontal stochastic wind velocity fields. Numerical examples fully reveal the validity and superiority of the proposed methods.

Keywords: stochastic wind velocity field; continuous proper orthogonal decomposition; frequency-wavenumber spectral representation; dimension reduction; non-uniform wavenumber intervals; FFT algorithm

1. Introduction

With the rapid development of technology and economy, a considerable number of complex engineering structures, such as high-rise buildings and long-span bridges, are constructed to satisfy the requirements of people's life and production in recent decades. Owing to the wind load is always the dominant design load of these complex structures, it is of paramount significance to proceed with the wind-induced dynamic response analysis for the performance-based design or control of these structures. Studies have shown that the dynamic responses of the structures subjected to the fluctuating wind load are extremely complicated, such as the structural along-wind vibration and the structural across-wind vibration (Khanduri *et al*. 1998, Zu and Lam 2018). In fact, the fluctuating wind load has randomness in nature (Huang *et al*. 2018, Zhu *et al*. 2018), which is generally described by the stochastic wind velocity field. Therefore, simulation of the stochastic wind velocity field is attracting increasing attention and no doubt to be the primary task in structural wind engineering.

Generally, the stochastic wind velocity field can be represented as the stationary multivariate stochastic process (the discrete form) or the stationary stochastic field (the continuous form). In practice, there are two widely-used methods for simulating the stationary multivariate stochastic processes, i.e., the spectral representation method (SRM) and the proper orthogonal decomposition (POD), of which are both based on the spectral decompositions of power spectral density (PSD) matrixes. The SRM was first proposed by Shinozuka (1971, 1972) in the application for simulating the multidimensional and multivariate stochastic processes (Wu *et al*. 2013, 2018). Then it was Yang (1972) who first successfully introduced the Fast Fourier Transform (FFT) algorithm to the SRM, and this treatment greatly enhances the computational efficiency when simulating the multivariate stochastic processes. Furthermore, Di Paola *et al*. (1998, 2001) proposed the POD and applied it to simulate the stochastic wind velocity processes. Compared with the SRM, the POD has explicit physical meanings. In addition, the model truncation technique can also be applied in the POD to accelerate the simulation with little loss of precision, which can be readily achieved by the first several modes possessing dominant energy (Chen and Letchford 2005, Huang 2015).

Although the theory and technology of the SRM and the POD have been well developed to date, it is still difficult to handle the issue when the simulated components rise to a large number (Benowitz and Deodatis 2015). In this case, the spectral decompositions may work slowly or even break down due to the adjacent points may exhibit a high degree

∗Corresponding author, Professor
E-mail: luhailin@wit.edu.cn
[a] Professor
E-mail: liuzhangjun@wit.edu.cn
[b] Ph.D. Candidate
E-mail: joehecg@163.com
[c] Ph.D. Candidate
E-mail: liuzenghuictgu@163.com

http://www.techno-press.com/journals/was&subpage=7 ISSN: 1226-6116 (Print), 1598-6225 (Online)

of correlation and the PSD matrix increasingly closes to singular as its order grows larger. Aiming at the above situation, Deodatis and Shinozuka (1989) then proposed the frequency-wavenumber spectral representation (FWSR) which expresses the stochastic field as a form of stochastic waves. Moreover, Benowitz and Deodatis (2015) combined the FWSR with the FFT algorithm and applied it in the simulation of horizontal stochastic wind velocity fields. Meanwhile, Carassale and Solari (2002) put forward a kind of continuous proper orthogonal decomposition (CPOD) to simulate the stochastic wind velocity fields based on the cross PSD functions, and gave the semi-analytical solution of the proper problem. Actually, the two continuous forms (FWSR and CPOD) can generate samples of arbitrary point along the main direction of structures, while the discrete forms can only obtain samples of a relatively small number of pre-assigned points. Consequently, in the refined dynamic response analysis for complex long-span and long-distance engineering structures with a series of numerous simulated points, the continuous forms should be preferred.

In practical applications, the random-phase-angles-based methods (Chen and Kareem 2005, Peng *et al*. 2016) associated with the above four representations are the most popular ones in the simulation of stochastic processes or fields. However, the random-phase-angles-based schemes all belong to the family of the conventional Monte Carlo methods which usually require millions of random phase angles uniformly distributed in the high-dimension space to ensure an acceptable simulation accuracy. As a result, this treatment will inevitably lead to the following two principle challenges. The first one is that the multitude of high-dimensional random variables cannot be obtained easily (Ghanem and Spanos 1991, Li and Chen 2009). At present, almost all pseudo random number generation method cannot commendably deal with the high-dimensional random variables. Though the accuracy of the Monte Carlo method is independent of the dimension of random variables in theory, there is still a great difficulty in generation of the pseudo random numbers. This can be attributed to the fact that the correlation of pseudo random numbers in different dimensions may be unexpectedly strong when the dimension is extremely high (Glasserman 2013, Chen *et al*. 2018). The second one is that due to the randomness of sampling caused by the Monte Carlo sampling method, each generated sample does not have an assigned probability and the samples cannot assemble a complete set in the probability level. This will result in the randomness of the dynamic system cannot be completely transmitted and evolved from the external excitations to structural dynamic responses. In fact, applying the Monte Carlo methods, only some statistics, such as mean, standard deviation and high order moments, can be obtained, while it is unavailable to capture accurate probability density functions of structural dynamic responses (Liu and Liu 2018). In view of this, it is of primary concern to reduce the number of the random variables without loss of accuracy and ensure the completeness of probability with respect to the generated samples.

In recent years, for the purpose of reducing the number of random variables, Chen *et al*. (2013, 2017) suggested the stochastic harmonic function representations of the stationary and non-stationary stochastic processes. Meanwhile, Liu *et al*. (2016) introduced the random function to the SRM, making it feasible to accurately represent the stationary and non-stationary stochastic processes with merely one or two elementary random variables. Utilizing the dimension reduction method of random function, the stationary multivariate stochastic processes can be naturally simulated by two or three elementary random variables (Liu *et al*. 2018a). The dimension reduction method bypassing the difficulties faced by the high-dimensional random variables can be combined with the probability density evolution method (PDEM) (Li and Chen 2009) to accurately evaluate the structural dynamic reliability (Liu and Liu 2018, Liu *et al.* 2018b, Liu *et al.* 2019). In this study, the dimension reduction method is extended in the simulation of the stochastic wind velocity fields using just one elementary random variable with several hundred representative points possessing assigned probabilities. Furthermore, this study also suggests an improved scheme with non-uniform wavenumber intervals to remarkably enhance the simulation efficiency and the PSD accuracy in low frequency component in the FWSR.

The specific contents of this study are organized as follows. The two original spectral representations of the stationary stochastic fields are firstly elicited in Section 2. And the relations between the CPOD and the FWSR are also expounded in this section. Following that, this study proposes a random function form including merely one elementary random variable, and introduces it to the CPOD and the FWSR to realize the dimension-reduction representations of the stochastic fields in Section 3. Meanwhile, to accelerate the numerical simulation, the application of the FFT algorithm is also discussed within this section. Furthermore, with the intention of improving the simulation efficiency and accuracy in the FWSR, the scheme with non-uniform wavenumber intervals embedded in the FFT algorithm is presented in Section 4. Then, the simulation of the horizontal stochastic wind velocity fields is carried out in Section 5, and the detailed comments of the CPOD and the FWSR are also exposed in this section. The superiority of the proposed dimension-reduction methods is fully demonstrated through the comparisons with the conventional Monte Carlo methods. Finally, some conclusions are summarized in Section 6.

2. Original spectral representations of stationary stochastic fields

Suppose that $f_0(x,t)$ is a zero-mean stationary stochastic field, it can be represented as the following Fourier-Stieltjes integral (Carassale and Solari 2002)

$$f_0(x,t) = \int_{-\infty}^{\infty} \mathrm{e}^{\mathrm{i}\omega t} \mathrm{d}Z_0(x,\omega) \tag{1}$$

where x and t denote the space variable and time variable, respectively; ω denotes the circular frequency; $\mathrm{i} = \sqrt{-1}$ denotes the imaginary unit; $Z_0(x,\omega)$ denotes a complex orthogonal stochastic field whose frequency increment

$\mathrm{d}Z_0(x,\omega)=Z_0(x,\omega+\mathrm{d}\omega)-Z_0(x,\omega)$ should satisfy the following basic conditions

$$E[\mathrm{d}Z_0(x,\omega)]=0\,;\quad \mathrm{d}Z_0(x,-\omega)=\mathrm{d}Z_0^*(x,\omega) \tag{2a}$$

$$E[\mathrm{d}Z_0(x,\omega)\mathrm{d}Z_0^*(x',\omega')]=S_{f_0}(x,x',\omega)\delta_{\omega\omega'}\mathrm{d}\omega \tag{2b}$$

where $E[\cdot]$ denotes the mathematical expectation; the superscript '$*$' denotes the complex conjugate; $S_{f_0}(x,x',\omega)$ denotes the two-sided cross PSD function in terms of the stochastic processes $f_0(x,t)$ and $f_0(x',t)$; $\delta_{\omega\omega'}$ denotes the Kronecker delta.

2.1 Continuous proper orthogonal decomposition (CPOD)

Let $\lambda_m(\omega)$ and $\psi_m(x,\omega)$ $(m=1,2,\cdots)$ be the eigenvalues and the eigenfunctions of the cross PSD function $S_{f_0}(x,x',\omega)$, respectively. In fact, they are the nontrivial solution of the second class Fredholm integral equation (Carassale and Solari 2002) expressed as

$$\int_\Omega S_{f_0}(x,x',\omega)\psi_m(x',\omega)\mathrm{d}x'=\lambda_m(\omega)\psi_m(x,\omega) \tag{3}$$

where Ω denotes the spatial domain.

In general, since the cross PSD function $S_{f_0}(x,x',\omega)$ is bounded, Hermitian and non-negative definite, its eigenvalues $\lambda_m(\omega)$ $(m=1,2,\cdots)$ are non-negative real functions and the corresponding eigenfunctions $\psi_m(x,\omega)$ $(m=1,2,\cdots)$ are complex functions of frequency ω. Further, $\lambda_m(\omega)$ and $\psi_m(x,\omega)$ should satisfy the following conditions

$$\int_\Omega \psi_i(x,\omega)\psi_j^*(x,\omega)\mathrm{d}x=\delta_{ij} \tag{4a}$$

$$\int_\Omega\int_\Omega S_{f_0}(x,x',\omega)\psi_i(x,\omega)\psi_j^*(x',\omega)\mathrm{d}x\mathrm{d}x'=\lambda_i(\omega)\delta_{ij} \tag{4b}$$

It is the completeness of the eigenfunctions $\psi_m(x,\omega)$ set that ensures the spectral decomposition of the cross PSD function (Kanwal 1971). In general, for a continuous stochastic field, there may be a finite or infinite number of eigenvalues. However, in either case, by means of sorting the eigenvalues in decreasing order, the cross PSD function thus can be approximately expressed as the sum of the first M_1 terms of eigenvalues containing dominant energy (Solari and Carassale 2001)

$$S_{f_0}(x,x',\omega)\approx\sum_{m=1}^{M_1}\lambda_m(\omega)\psi_m(x,\omega)\psi_m^*(x',\omega) \tag{5}$$

where M_1 denotes the truncation number of eigenvalues, depending on the truncation accuracy which is defined as the ratio of the sum of the first M_1 terms of eigenvalues to the sum of total eigenvalues.

Combining Eq. (5) and Eq. (2(b)), the frequency increment $\mathrm{d}Z_0(x,\omega)$ can be approximately expressed as the following discrete form

$$\begin{aligned}\mathrm{d}Z_0(x,\omega)\big|_{\omega=\omega_n}&\approx\Delta Z_0(x,\omega_n)\\&=\sum_{m=1}^{M_1}\sqrt{\lambda_m(\omega_n)\Delta\omega}\,\psi_m(x,\omega_n)P_{mn}\end{aligned} \tag{6a}$$

$$\omega_n=\begin{cases}(n-0.5)\Delta\omega & n=1,2,\cdots,N\\(n+0.5)\Delta\omega & n=-1,-2,\cdots,-N\end{cases} \tag{6b}$$

where $\Delta\omega=\omega_\mathrm{u}/N$ is the frequency interval, in which ω_u is the upper-cutoff frequency and N is the number of frequency intervals; P_{mn} denotes the zero-mean complex orthogonal random variables.

It should be noted that the frequency interval $\Delta\omega$ should be small enough to ensure the validity of the approximate representation in Eq. (6(a)), meanwhile, the corresponding time interval Δt should satisfy the following condition (Shinozuka and Deodatis 1996)

$$\Delta t\le\frac{\pi}{\omega_\mathrm{u}} \tag{7}$$

For convenience, the complex eigenfunctions $\psi_m(x,\omega_n)$ and the complex orthogonal random variables P_{mn} can be defined as the following real form, respectively

$$\psi_m(x,\omega_n)=\chi_m(x,\omega_n)-\mathrm{i}\gamma_m(x,\omega_n) \tag{8a}$$

$$P_{mn}=R_{mn}-\mathrm{i}I_{mn} \tag{8b}$$

where R_{mn} and I_{mn} denote the real orthogonal random variables satisfying the following conditions

$$E[R_{mn}]=E[I_{mn}]=0\,;\quad E[R_{im}I_{jn}]=0 \tag{9a}$$

$$E[R_{im}R_{jn}]=E[I_{im}I_{jn}]=\frac{1}{2}\delta_{ij}\delta_{mn} \tag{9b}$$

where $i=1,2,\cdots,M_1$; $j=1,2,\cdots,N$.

Generally, the eigenvalues have symmetry with respect to the frequency, i.e., $\lambda_m(\omega_n)=\lambda_m(-\omega_n)$; and the eigenfunctions satisfy the relation $\psi_m(x,-\omega_n)=\psi_m^*(x,\omega_n)$. Therefore, based on Eqs. (6) and (8), the original stochastic field $f_0(x,t)$ can be approximately expressed as the following simplified real form

$$\begin{aligned}f_1(x,t)=2\sum_{m=1}^{M_1}\sum_{n=1}^{N}\sqrt{\lambda_m(\omega_n)\Delta\omega}\,\cdot\\\big\{\chi_m(x,\omega_n)\big[R_{mn}\cos(\omega_n t)+I_{mn}\sin(\omega_n t)\big]+\\\gamma_m(x,\omega_n)\big[R_{mn}\sin(\omega_n t)-I_{mn}\cos(\omega_n t)\big]\big\}\end{aligned} \tag{10}$$

where $f_1(x,t)$ denotes the original spectral representation based on the CPOD. The paper will use the CPOD to name Eq. (10) hereinafter.

From the above process, it can be observed that the CPOD expresses the stochastic field as the summation of the first M_1 terms of the proper modes. The eigenvalues represent the energy contained in the proper modes, and the eigenfunctions, which are the continuous functions of the space coordinates x, determine the mode shapes of the proper modes. In addition, it should be noted that Eq. (10) cannot be directly used in the simulation of stochastic field since the probability distributions of the orthogonal random variables R_{mn} and I_{mn} are undetermined.

2.2 Frequency-wavenumber spectral representation (FWSR)

In Eq. (1), if we define

$$\mathrm{d}Z_0(x,\omega)=\int_{-\infty}^{\infty}\mathrm{e}^{\mathrm{i}\kappa x}\mathrm{d}Z_1(\kappa,\omega) \tag{11}$$

Thus, the stationary and homogeneous stochastic field $f_0(x,t)$ can be expressed as (Priestley 1965, Deodatis and Shinozuka 1989)

$$f_0(x,t)=\int_{-\infty}^{\infty}\int_{-\infty}^{\infty}\mathrm{e}^{\mathrm{i}(\kappa x+\omega t)}\mathrm{d}Z_1(\kappa,\omega) \tag{12}$$

where κ denotes the wavenumber corresponding to the spatial variable x; the increment $\mathrm{d}Z_1(\kappa,\omega)=Z_1(\kappa+\mathrm{d}\kappa,\omega+\mathrm{d}\omega)-Z_1(\kappa,\omega)$ should satisfy the following conditions

$$E[\mathrm{d}Z_1(\kappa,\omega)]=0\,;\quad \mathrm{d}Z_1(-\kappa,-\omega)=\mathrm{d}Z_1^*(\kappa,\omega) \tag{13a}$$

$$E[\mathrm{d}Z_1(\kappa,\omega)\mathrm{d}Z_1^*(\kappa',\omega')]=S_{\mathrm{w}}(\kappa,\omega)\delta_{\kappa\kappa'}\delta_{\omega\omega'}\mathrm{d}\kappa\mathrm{d}\omega \tag{13b}$$

where $S_{\mathrm{w}}(\kappa,\omega)$ denotes the two-sided frequency-wavenumber spectral density (FSD) function of $f_0(x,t)$, generally satisfying the following symmetry, i.e., $S_{\mathrm{w}}(\kappa,\omega)=S_{\mathrm{w}}(\pm\kappa,\pm\omega)$ described in (Shinozuka and Deodatis 1996).

For stationary and homogeneous stochastic field, the complex increment $\mathrm{d}Z_1(\kappa,\omega)=\mathrm{d}U(\kappa,\omega)-\mathrm{i}\mathrm{d}V(\kappa,\omega)$. Thus, the real orthogonal increments $\mathrm{d}U(\kappa,\omega)$ and $\mathrm{d}V(\kappa,\omega)$ can be approximately written as the following discrete form, respectively

$$\begin{aligned}\mathrm{d}U(\kappa,\omega)\Big|_{\kappa=\kappa_m,\omega=\omega_n}&\approx\Delta U^{(i)}(\kappa_m,\omega_n)\\&=\sqrt{S_{\mathrm{w}}(\kappa_m,\omega_n)\Delta\kappa\Delta\omega}X_{mn}^{(i)},\ i=1,2\end{aligned} \tag{14a}$$

$$\begin{aligned}\mathrm{d}V(\kappa,\omega)\Big|_{\kappa=\kappa_m,\omega=\omega_n}&\approx\Delta V^{(i)}(\kappa_m,\omega_n)\\&=\sqrt{S_{\mathrm{w}}(\kappa_m,\omega_n)\Delta\kappa\Delta\omega}Y_{mn}^{(i)},\ i=1,2\end{aligned} \tag{14b}$$

where $X_{mn}^{(i)}$ and $Y_{mn}^{(i)}$ $(i=1,2)$ are the zero-mean real orthogonal random variables which satisfy Eq. (15(a)); ω_n is equally defined in Eq. (6(b)), and κ_m is defined in Eq. (15(b)), such that

$$E[X_{mn}^{(i)}]=E[Y_{mn}^{(i)}]=0\,;\quad E[X_{km}^{(i)}Y_{ln}^{(j)}]=0 \tag{15a}$$

$$E[X_{km}^{(i)}X_{ln}^{(j)}]=E[Y_{km}^{(i)}Y_{ln}^{(j)}]=\frac{1}{2}\delta_{ij}\delta_{kl}\delta_{mn} \tag{15b}$$

$$\kappa_m=\begin{cases}(m-0.5)\Delta\kappa & m=1,2,\cdots,M_2\\(m+0.5)\Delta\kappa & m=-1,-2,\cdots,-M_2\end{cases} \tag{15c}$$

where $i,j=1,2$; $\Delta\kappa=\kappa_{\mathrm{u}}/M_2$ denotes the wavenumber interval, in which κ_{u} is the upper-cutoff wavenumber, and M_2 is the number of the wavenumber intervals.

Substituting Eq. (14) into Eq. (12), thus the original stochastic field $f_0(x,t)$ can be approximately rewritten as the following discrete form

$$\begin{aligned}f_2(x,t)=2\sum_{m=1}^{M_2}\sum_{n=1}^{N}\sqrt{S_{\mathrm{w}}(\kappa_m,\omega_n)\Delta\kappa\Delta\omega}\,\cdot\\ \left\{[\cos(\kappa_m x+\omega_n t)X_{mn}^{(1)}+\sin(\kappa_m x+\omega_n t)Y_{mn}^{(1)}]+\right.\\ \left.[\cos(-\kappa_m x+\omega_n t)X_{mn}^{(2)}+\sin(-\kappa_m x+\omega_n t)Y_{mn}^{(2)}]\right\}\end{aligned} \tag{16}$$

where $f_2(x,t)$ is the so-called original spectral representation based on the FWSR.

It is noted that $\Delta\omega$ and $\Delta\kappa$ should be small enough to ensure that Eq. (12) can be replaced by Eq. (16) without loss of accuracy. Similarly, the time interval Δt must satisfy the condition defined in Eq. (7), the corresponding spatial interval Δx must satisfy the analogical condition expressed as

$$\Delta x\leq\frac{\pi}{\kappa_{\mathrm{u}}} \tag{17}$$

The FWSR represents the stationary and homogeneous stochastic field as the sum of a series of stochastic waves modulated by the random variables. In addition, the FSD function can also be regarded as the energy distribution in the two-dimensional domain of frequency and wavenumber, while the modulation function with respect to the spatial variables x is contained in the cosine function. Similarly, due to the probability distributions of $X_{mn}^{(i)}$ and $Y_{mn}^{(i)}$ $(i=1,2)$ are unknown, one can not directly utilize Eq. (16) to generate representative samples either.

2.3 Relations between the CPOD and the FWSR

It can be observed from Eq. (10) and Eq. (16) that the above two original spectral representations have similar formats, say both express the stochastic field as summation of a series of products upon the trigonometric functions and the energy elements which denote the energy distribution of the stochastic field. In fact, the above two representations are equivalent in certain circumstances.

For examples, considering a zero-mean stationary and homogeneous stochastic field $\bar{f}_1(x,t)$ with period L in space domain and period T in time domain, and taking one period from which defined in the space domain $-L/2 \le x \le L/2$ and the time domain $-T/2 \le t \le T/2$, the relations between the two representations were summarized by Chen and Kareem (2005) as follows.

The eigenfunctions $\psi_m(x,\omega)$ $(m = \pm 1, \pm 2, \cdots)$ of the CPOD are identical to the following Fourier basis functions

$$\psi_m(x,\omega) = \frac{1}{\sqrt{L}} \mathrm{e}^{\mathrm{i}\kappa_m x} \tag{18}$$

Then the corresponding eigenvalues become the PSD functions expressed as

$$\lambda_m(\omega) = \int_{-L/2}^{L/2} S_{f_0}(\xi,\omega) \mathrm{e}^{\mathrm{i}\kappa_m \xi} \mathrm{d}\xi = 2\pi S_{\mathrm{w}}(\kappa_m,\omega) \tag{19}$$

where $\xi = x - x'$ denotes the spatial distance between the points x and x', thus $S_{f_0}(\xi,\omega)$ is equal to $S_{f_0}(x,x',\omega)$. And the integral result can be readily obtained by the relation between the PSD function and the FSD function.

Hence, utilizing Eqs. (18) and (19) and defining $\Delta\kappa = 2\pi/L$, the stochastic field $\bar{f}_1(x,t)$ based on the CPOD can be rewritten as

$$\begin{aligned} \bar{f}_1(x,t) = 2\sum_{m=1}^{M}\sum_{n=1}^{N} \sqrt{S_{\mathrm{w}}(\kappa_m,\omega_n)\Delta\kappa\Delta\omega} \cdot \\ \left\{ \left[R_{mn}\cos(\kappa_m x + \omega_n t) + I_{mn}\sin(\kappa_m x + \omega_n t) \right] + \right. \\ \left. \left[R_{-mn}\cos(-\kappa_m x + \omega_n t) + I_{-mn}\sin(-\kappa_m x + \omega_n t) \right] \right\} \end{aligned} \tag{20}$$

where M is equal to M_1 in the CPOD defined in Eq. (10).

Certainly, M in Eq. (20) can also be equal to M_2 in the FWSR. It is obvious that in this case the above two original spectral representations are totally identical, say Eq. (20) based on the CPOD is exactly equal to Eq. (16) based on the FWSR, and the two can be transformed to each other easily. In fact, the two original spectral representations have similar meanings. On the one hand, as previously mentioned, the CPOD has an explicit physical meaning. The eigenvalues refer to the energy of the proper modes, and the original stochastic field can be accurately simulated by the first M_1 terms of the eigenvalues containing the dominant energy. On the other hand, similar to eigenvalues, the FSD functions can be rewritten as linear functions of eigenvalues, which is reflected in Eq. (19), and represent the energy distribution of the stochastic field in the two-dimensional region of frequency and wavenumber.

Though the two original spectral representations can be transformed to each other in form, they are significantly different in essence, mainly reflected in the following two aspects.

i) Eq. (20) is a special case of Eq. (10) in essence. For homogeneous stochastic field $\bar{f}_1(x,t)$ or $f_2(x,t)$ with spatial period L, the spatial domain is generally defined in the whole space, i.e., $-\infty < x < \infty$. In this way, the eigenfunctions and eigenvalues of the stochastic fields are defined as Eqs. (18) and (19), respectively. However, in practice application, the stochastic field is bounded in space, generally defined in $0 \le x \le L$, even if it may lead to the non-completely homogeneous stochastic field. At this point, the explicit expressions of eigenvalues and eigenfunctions can be directedly obtained by solving the proper problem defining as Eq. (3). Therefore, it is believed that, as for the stationary and homogeneous stochastic field, the FWSR can be considered as a priority. However, the CPOD can provide an optimal representation for the non-completely homogeneous stochastic field.

ii) The other difference is the number of random variables in the two original spectral representations. The CPOD just requires $2 \times M_1 \times N$ orthogonal random variables, but the number in the FWSR is $4 \times M_2 \times N$. This is owing to that for any specified space coordinate, the eigenvalues and the eigenfunctions are unary functions of frequency, and the frequency increment $\mathrm{d}Z_0(x,\omega)$ has symmetry about the ω axis. However, the FSD functions are binary functions of frequency and wavenumber, the increment $\mathrm{d}Z_1(\kappa,\omega)$ is symmetric about the original point of the frequency-wavenumber two-dimensional region. What's more, $8 \times M \times N$ or $8 \times M_y \times M_z \times N$ orthogonal random variables are even required in the case that the joint wavenumber-frequency spectral density functions are ternary functions (Song *et al*. 2018).

3. Dimension-reduction simulation of stationary stochastic field

As afore-mentioned, the first task when utilizing Eq. (10) or Eq. (16) to simulate the stochastic field is to determine the probability distributions of the random variables. In fact, arbitrary probability distribution is theoretically effective. Generally, the conventional Monte Carlo methods regard the random variables as the random phase angles uniformly distributed in $[0, 2\pi]$, such that only a half number of random variables compared with the original spectral representations is required. However, due to the number of random variables in Eqs. (10) and (16) is always as high as millions, the conventional Monte Carlo methods still has to face the dilemma caused by the high-dimensional random numbers. Moreover, since the Monte Carlo sampling method is random in essence and the random variables require to be reselected to generate a new sample each time, the probability of each generated sample is unknown. Consequently, it is unfeasible to obtain the accurate probability density functions with respect to the dynamic responses of complex engineering structures under stochastic excitations. For that, this study introduces the idea of random function to effectively reduce the dimension of random variables, and applies it in the simulation of stochastic fields, making it possible to implement the refined dynamic response analysis and dynamic reliability assessment of complex engineering structures combining with the PDEM.

3.1 Random function representation of the orthogonal random variables

In the previous works, Liu *et al*. (2018a) successfully constructed random functions using merely two or three elementary random variables with representative points owing given probabilities to realize the efficient dimension-reduction simulation of stationary random processes. As a matter of fact, the dimension of random variables can be further reduced to just one, which will be presented in this section. The specific implementation procedures are as follows.

Step 1, construct orthogonal functions

At first, for simplicity, suppose $R_{mn}=X_{mn}^{(1)}$ and $I_{mn}=Y_{mn}^{(1)}$ since they satisfy the same conditions respectively defined in Eqs. (9) and (15(a)). Then, construct the orthogonal random variables set $\{\bar{X}_{pq}^{(j)},\bar{Y}_{pq}^{(j)}\}$ $(j=1,2)$ utilizing merely one elementary random variable, such that

$$\bar{X}_{pq}^{(j)}(\theta)=\cos(r\theta),\ j=1,2 \tag{21a}$$

$$\bar{Y}_{pq}^{(j)}(\theta)=\sin(r\theta),\ j=1,2 \tag{21b}$$

where θ follows uniform distribution in the range $[0,2\pi]$; $r=h(j,p,q)$ satisfies the conditions as follows

i) $p=1,2,\cdots,M$ and $q=1,2,\cdots,N$, where M is the same as that in Eq. (20).

ii) There is just one set $\{j,p,q\}$ corresponding to the specific value of $h(j,p,q)$,i.e., the equation $h(i,k,l)=h(j,p,q)$ exists only in the case that i = j, k = p and l = q.

iii) It is recommended that $r=h(j,p,q)$ takes an integer.

In the present paper, we can define $r=[(j-1)\times N+q-1]\times M+p$. Obviously, the orthogonal functions defined in Eq. (21) completely satisfy the conditions defined in Eq. (15(a)). The similar proof process for the constructed random functions has been elaborated by Liu *et al*. (2018a), which will not be detailed herein.

Step 2, construct one-to-one mapping relationships

Then, the order of the terms in the orthogonal variables set $\{\bar{X}_{pq}^{(j)},\bar{Y}_{pq}^{(j)}\}$ $(j=1,2)$ constructed in Step 1 requires to be messed up to obtain the target orthogonal random variables set $\{X_{mn}^{(i)},Y_{mn}^{(i)}\}$ $(i=1,2)$ through a unique transformation. The one-to-one mapping between the two sets can be realized by the MATLAB tool box functions $rand('state',0)$ and $temp=randperm(2M\times N)$. Suppose that the $2\times M\times N$-order matrixes $\mathbf{X}$ and $\bar{\mathbf{X}}$ denote the sets $X_{mn}^{(j)}$ and $\bar{X}_{pq}^{(j)}$ $(j=1,2)$, respectively. Then defining index tags $c=[(i-1)\times N+(n-1)]\times M+m$ and $\bar{c}=[(j-1)\times N+(q-1)]\times M+p$, the one-to-one mapping relationship can thus be expressed as follows

$$\mathbf{X}[c]=\bar{\mathbf{X}}[temp(c)]=\bar{\mathbf{X}}[\bar{c}] \tag{22}$$

The other random variables $Y_{mn}^{(i)}$ $(i=1,2)$ can be realized in the same way. Obviously, the essence of Eq. (22) is to stochastically rearrange the random variables defined in Eq. (21). Thus, the target orthogonal random variables set $\{X_{mn}^{(i)},Y_{mn}^{(i)}\}$ $(i=1,2)$ using merely one elementary random variable are finally obtained.

Step 3, substitute the random functions into the original spectral representations

Substituting $\{X_{mn}^{(1)},Y_{mn}^{(1)}\}$ into Eq. (10) and utilizing the trigonometric formulas to simplify the equation, then the dimension-reduction representation of the CPOD is expressed as

$$\tilde{f}_1(x,t)=2\sum_{m=1}^{M_1}\sum_{n=1}^{N}\psi_m(x,\omega_n)\sqrt{\lambda_m(\omega_n)\Delta\omega}\cdot \cos\left[\omega_n t+\phi_m(x,\omega_n)-\varphi_{mn}^{(1)}(\theta)\right] \tag{23}$$

where $\phi_m(x,\omega_n)=\arctan\left[\gamma_m(x,\omega_n)/\chi_m(x,\omega_n)\right]$; the random phase $\varphi_{mn}^{(i)}(\theta)=\bar{\varphi}_{pq}^{(j)}(\theta)=r\times\theta$ $(i,j=1,2)$, and the one-to-one mapping relationship between $\varphi_{mn}^{(i)}(\theta)$ and $\bar{\varphi}_{pq}^{(j)}(\theta)$ is identical to that between $X_{mn}^{(i)}$ $(i=1,2)$ and $\bar{X}_{pq}^{(j)}$ $(j=1,2)$.

Similarly, the original stochastic field based on the FWSR can be rewritten as the following dimension-reduction form

$$\tilde{f}_2(x,t)=2\sum_{m=1}^{M_2}\sum_{n=1}^{N}\sqrt{S_{\mathrm{w}}(\kappa_m,\omega_n)\Delta\kappa\Delta\omega}\cdot \left\{\cos[\kappa_m x+\omega_n t-\varphi_{mn}^{(1)}(\theta)]+\cos[-\kappa_m x+\omega_n t-\varphi_{mn}^{(2)}(\theta)]\right\} \tag{24}$$

It can be seen that the proposed dimension-reduction schemes have similar simulation formulations with the conventional Monte Carlo schemes involving the random phase angles. However, it is worth noting that the dimension of random variables between the two schemes varies considerably. Specifically, the randomness dimension in the conventional Monte Carlo schemes is $M_1\times N$ or $2\times M_2\times N$, however, that in the proposed methods is just one, which could effectively avoid the difficulties of dealing with the high-dimensional random variables. Treated in this way, the one-dimensional representative point sets can thus be readily obtained by some well-developed sampling methods, such as the number theoretical method. Benefiting from this, each generated representative sample has an assigned probability and all the representative samples assemble a complete set in the probability level, providing a handy combination with the PDEM to perform the accurate dynamic response analysis and dynamic reliability evaluation of randomly-excited complex engineering structures.

3.2 Simulation scheme with FFT algorithm

Though the high dimension of random variables is effectively reduced employing Eqs. (23) and (24), it still results in expense in computational effort and time due to the huge number of frequency and wavenumber terms. Hence, a particular effort is made in this study to efficiently expedite the numerical simulation by means of adopting the FFT algorithm. In conjunction with the FFT algorithm, Eq. (23) can be rewritten as

$$\tilde{f}_1(x, q_1\Delta t) = \mathrm{Re}\left[\sum_{m=1}^{M_1} B_{mq_2} \exp\left(\frac{\mathrm{i}q_1\pi}{2N}\right)\right] \tag{25a}$$

$$B_{mq_2} = \sum_{n=1}^{2N} A_{mn} \exp\left[\frac{\mathrm{i}(n-1)q_2\pi}{N}\right] \tag{25b}$$

$$\begin{aligned} A_{mn} &= 2\left|\psi_m(x,\omega_n)\right|\sqrt{\lambda_m(\omega_n)\Delta\omega}\cdot \\ &\exp\left\{\mathrm{i}[\phi_m(x,\omega_n) - \varphi_{mn}^{(1)}(\theta)]\right\} \end{aligned} \tag{25c}$$

where q_2 denotes the remainder of $q_1/2N$, $q_1 = 0,1,\cdots,2\times M_1\times N-1$, $q_2 = 0,1,\cdots,2N-1$; $\mathrm{Re}[\cdot]$ denotes the real part. Eq. (25(c)) is true once $0 < n \le N$, while $A_{mn} = 0$ if $N < n \le 2N$.

Similarly, the dimension-reduction FWSR combining with the FFT algorithm can be expressed as the following form

$$\begin{aligned} \tilde{f}_2(p_1\Delta x, q_1\Delta t) = \mathrm{Re}\Bigg\{ &\exp\left[\frac{\mathrm{i}p_1\pi}{2M_2} + \frac{\mathrm{i}q_1\pi}{2N}\right] C_{p_2q_2}^{(1)} + \\ &\exp\left[-\frac{\mathrm{i}p_1\pi}{2M_2} + \frac{\mathrm{i}q_1\pi}{2N}\right] C_{p_2q_2}^{(2)} \Bigg\} \end{aligned} \tag{26a}$$

$$C_{p_2q_2}^{(j)} = \sum_{m=1}^{2M_2}\sum_{n=1}^{2N} D_{nm}^{(j)} \exp\left[\frac{\mathrm{i}(m-1)p_2\pi}{M_2}(-1)^{j-1} + \frac{\mathrm{i}(n-1)q_2\pi}{N}\right] \tag{26b}$$

$$D_{mn}^{(j)} = 2\sqrt{S_{\mathrm{w}}(\kappa_m,\omega_n)\Delta\kappa\Delta\omega}\exp\left[-\mathrm{i}\times\varphi_{mn}^{(j)}(\theta)\right] \tag{26c}$$

where p_2 denotes the remainder of $p_1/(2M_2)$, $p_1 = 0,1,\cdots,2\times M_2\times N-1$, $p_2 = 0,1,\cdots,2M_2-1$; q_2 denotes the remainder of $q_1/(2N)$, $q_1 = 0,1,\cdots,2\times M_2\times N-1$, $q_2 = 0,1,\cdots,2N-1$; $j=1,2$. Similarly, Eq. (26(c)) is true if $0 < m \le M_2, 0 < n \le N$.

It can be observed from Eqs. (25) and (26) that the FFT algorithm can only be adopted for frequency terms in the CPOD, whereas the FFT algorithm can be applied for both frequency and wavenumber terms in the FWSR, resulting in the FWSR owes a relatively higher simulation efficiency for the sample generation of a stochastic field with numerous simulated points.

4. An improved scheme using non-uniform wavenumber intervals

In wind engineering, in consideration of the fairly large error of the PSD function in low frequency and the poor simulation efficiency in the FWSR (Benowitz and Deodatis 2015), an improved scheme involving the non-uniform wavenumber intervals is proposed. According to the convergence rule of the FSD function upon wavenumber, this study adopts two wavenumber intervals to expound the validity of the scheme, say the minor wavenumber interval $\Delta\kappa_1$ used in low wavenumber component and the major wavenumber interval $\Delta\kappa_2$ used in high wavenumber component. Suppose $M_3^{(1)}$ and $M_3^{(2)}$ denote the numbers of the wavenumber intervals $\Delta\kappa_1$ and $\Delta\kappa_2$, respectively. And $M_3 = M_3^{(1)} + M_3^{(2)}$ denotes the total number of wavenumber intervals. Thus, the wavenumber κ_m in this case is defined as

When $m = 1,2,\cdots,M_3^{(1)}$

$$\kappa_m = (m-0.5)\Delta\kappa_1 \tag{27a}$$

When $m = M_3^{(1)}+1,\cdots,M_3$

$$\kappa_m = (M_3^{(1)}-0.5)\Delta\kappa_1 + (m - M_3^{(1)} - 0.5)\Delta\kappa_2 \tag{27b}$$

In fact, this scheme can also be combined with the FFT algorithm. Thus, the stochastic field based on non-uniform wavenumber intervals can be expressed as

$$\begin{aligned} \hat{f}_2(x,t) = \mathrm{Re}\Bigg\{ &\exp\left[\frac{\mathrm{i}p_1\pi}{2M_3^{(1)}} + \frac{\mathrm{i}q_1\pi}{2N}\right] C_{p_2q_2}^{(1)} + \exp\left[\frac{\mathrm{i}}{2}\left[\left(2M_3^{(1)}-1\right)\Delta\kappa_1 + \Delta\kappa_2\right] p_1'\Delta x_2 + \frac{\mathrm{i}q_1\pi}{2N}\right] C_{p_2'q_2}^{(3)} + \\ &\exp\left[-\frac{\mathrm{i}p_1\pi}{2M_3^{(1)}} + \frac{\mathrm{i}q_1\pi}{2N}\right] C_{p_2q_2}^{(2)} + \exp\left[-\frac{\mathrm{i}}{2}\left[\left(2M_3^{(1)}-1\right)\Delta\kappa_1 + \Delta\kappa_2\right] p_1'\Delta x_2 + \frac{\mathrm{i}q_1\pi}{2N}\right] C_{p_2'q_2}^{(4)} \Bigg\} \end{aligned} \tag{28a}$$

$$C_{p_2q_2}^{(j)} = \sum_{m=1}^{2M_3^{(1)}}\sum_{n=1}^{2N} D_{mn}^{(j)} \exp\left[\frac{\mathrm{i}(m-1)p_2\pi}{M_3^{(1)}}(-1)^{j-1} + \frac{\mathrm{i}(n-1)q_2\pi}{N}\right] \tag{28b}$$

$$D_{mn}^{(j)} = \begin{cases} 2\sqrt{S_{\mathrm{w}}(\kappa_m,\omega_n)\Delta\kappa_1\Delta\omega}\exp[-\mathrm{i}\times\varphi_{mn}^{(j)}(\theta)] & 0 < m \le M_3^{(1)}, 0 < n \le N \\ 0 & \text{otherwise} \end{cases} \tag{28c}$$

$$C_{p_2' q_2}^{(j+2)} = \sum_{m=1}^{2M_3^{(2)}} \sum_{n=1}^{2N} D_{mn}^{(j+2)} \exp\left[\frac{\mathrm{i}(m-1)p_2'\pi}{M_3^{(2)}}(-1)^{j-1} + \frac{\mathrm{i}(n-1)q_2\pi}{N}\right] \tag{28d}$$

$$D_{mn}^{(j+2)} = \begin{cases} 2\sqrt{S_{\mathrm{w}}(\kappa_m, \omega_n)\Delta\kappa_2\Delta\omega}\exp[-\mathrm{i}\times\varphi_{mn}^{(j)}(\theta)] & M_3^{(1)} < m \le M_3, 0 < n \le N \\ 0 & \text{otherwise} \end{cases} \tag{28e}$$

where $j = 1, 2$; p_2' denotes the remainder of $p_1'/(2M_3^{(2)})$, $p_1' = 0, 1, \cdots, 2\times M_3^{(2)} \times N - 1$, $p_2' = 0, 1, \cdots, 2M_3^{(2)} - 1$.

At this point, it is necessary to state that Eq. (28) can be conveniently realized in practice applications regardless of their complex forms. As a matter of fact, the wavenumber can be dispersed by means of more wavenumber intervals, and the frequency can also be treated in the same way, in theory which can significantly improve the accuracy and efficiency of the FWSR. However, due to the length of this study confined, the elaboration will not be expanded here. In addition, it is of great significance that in theory the proposed scheme involving the non-uniform frequency intervals can be also applied in the CPOD, even the POD and the SRM, which shows that it has a broad application prospect.

To distinguish the above three representations, say Eqs. (25), (26) and (28), they are named DR-CPOD, DR-FWSR-I and DR-FWSR-II, respectively. The availability of the proposed methods scrutinized by numerical examples will be presented in the next section.

5. Numerical example of horizontal stochastic wind velocity fields

5.1 The semi-analytical solutions of proper problem in CPOD and the explicit FSD function in FWSR

Obviously, in the CPOD, the paramount work for simulating the stochastic wind velocity field is to solve the second class Fredholm integral equation defined in Eq. (3); while in the FWSR, it is to obtain the explicit expression of FSD function, which are discussed in the following sections.

5.1.1 The eigenvalues and eigenfunctions

Generally, in wind engineering, as for the stochastic field defined in the horizontal spatial domain $0 \le x \le L$ and the time domain $0 \le t \le T$, the cross PSD function of which can be defined as follows

$$S_{f_0}(\xi, \omega) = S_0(\omega) \times Coh(\xi, \omega) \tag{29}$$

where $S_0(\omega)$ denotes the two-sided auto PSD function of the stochastic field; $Coh(\xi, \omega)$ denotes the spatial coherence function. In this study, $Coh(\xi, \omega)$ adopts the Davenport spatial coherence function expressed as (Davenport 1961, Peng *et al*. 2018)

$$Coh(\xi, \omega) = \exp\left[-\frac{\alpha(\omega)|\xi|}{L}\right] \tag{30}$$

where $\alpha(\omega) = (c_x L|\omega|)/(2\pi\bar{u}_z)$; c_x is the decay factor along the horizontal direction, valued by $c_x = 10$ in this study; $\bar{u}_z$ is the average wind velocity at the height *z*.

Utilizing the Davenport spatial coherence function, Carassale and Solari (2002) derived the following semi-analytic expressions of the eigenvalues and eigenfunctions from the second class Fredholm integral equation

$$\lambda_m(\omega) = \frac{2L\alpha(\omega)S_0(\omega)}{\mu_m^2 + \alpha^2(\omega)} \tag{31a}$$

$$\psi_m(x, \omega) = \frac{\alpha(\omega)}{\sqrt{\mu_m^2 + \alpha^2(\omega) + 2\alpha(\omega)}}\sqrt{\frac{2}{L}} \cdot \left[\sin\left(\frac{\mu_m x}{L}\right) + \frac{\mu_m}{\alpha(\omega)}\cos\left(\frac{\mu_m x}{L}\right)\right] \tag{31b}$$

where $\psi_m(x, \omega)$ is real, which means $\phi_m(x, \omega_n)$ in Eq. (23) is equal to zero. The parameter μ_m can be obtained by the following equation

$$\left[\tan(\mu_m/2) + \frac{\mu_m}{\alpha(\omega)}\right]\left[\tan(\mu_m/2) - \frac{\alpha(\omega)}{\mu_m}\right] = 0 \tag{32}$$

It is obvious that the parameter μ_m only depends on the parameter $\alpha(\omega)$. In practice, on the basis of the periodicity of the tangent function, the dichotomy can be applied to obtain the approximate solution of μ_m. In addition, it is worth mentioning that the eigenfunctions have the symmetry or anti-symmetry about the midpoint $x = L/2$ in the space domain $0 \le x \le L$. In the case of $\tan(\mu_m/2) = \alpha(\omega)/\mu_m$, the eigenfunctions are symmetric about the midpoint; in the case of $\tan(\mu_m/2) = -\mu_m/\alpha(\omega)$, the eigenfunctions have anti-symmetry about the midpoint, which is concordant to the structural vibration modes in structural dynamics.

5.1.2 The explicit expression of FSD function

In the FWSR, the relation between the FSD function and PSD function can be expressed as (Zerva 1992)

$$S_{\mathrm{w}}(\kappa,\omega)=\frac{1}{2\pi}\int_{-\infty}^{\infty}S_{f_0}(\xi,\omega)\mathrm{e}^{-\mathrm{i}\kappa\xi}\mathrm{d}\xi \tag{33}$$

Owing to the Davenport coherence function is adopted as expressed in Eq. (30), Eq. (33) can be further expressed as the following form (Benowitz and Deodatis 2015)

$$S_{\mathrm{w}}(\kappa,\omega)=\frac{1}{2\pi}S_0(\omega)F(\kappa,\omega) \tag{34a}$$

$$F(\kappa,\omega)=\int_{-\infty}^{\infty}Coh(\xi,\omega)\mathrm{e}^{-\mathrm{i}\kappa\xi}\mathrm{d}\xi=\frac{c_x\,|\,\omega\,|}{\pi\bar{u}_z\left[\kappa^2+\left(\dfrac{c_x\,|\,\omega\,|}{2\pi\bar{u}_z}\right)^2\right]} \tag{34b}$$

Thus, the FSD function of horizontal stochastic wind velocity field is expressed explicitly. Notice that the FSD function is inversely proportional to the wavenumber, which has consistency of convergent rule of the eigenvalue $\lambda_m(\omega)$ defined in Eq. (31(a)).

It is worth mentioning that there is a limitation in the application of the CPOD, say the semi-analytical solutions defined by Eqs. (31) and (32) are only applicable to the cross PSD function independent of altitude *z*. However, the FWSR can be applied in arbitrary one-dimensional-space stochastic wind velocity field, say no matter the wind velocity field is vertical or horizontal. What's more, the FWSR can represent two-dimensional-space stochastic fields by introducing new wavenumber in other directions (Song *et al*. 2018), indicating that the FWSR has a wider range of applications in the simulation of stochastic fields.

5.2 Numerical examples

For the purpose of verifying the validity of the proposed dimension-reduction methods, this study performs a simulation of the horizontal stochastic wind velocity fields acting on a long-span bridge. The simulation parameters are listed in Table 1.

Moreover, the most generally used two-sided Kaimal fluctuating wind velocity spectrum is applied in this study to describe the characteristics of the horizontal stochastic wind velocity field, given by (Kaimal *et al.* 1972)

$$S_0(\omega)=\frac{200u_*^2z}{4\pi\bar{u}_z}\frac{1}{(1+50\bar{\omega})^{5/3}} \tag{35a}$$

$$\bar{\omega}=\frac{\omega z}{2\pi\bar{u}_z};\ u_*=\frac{K\bar{u}_z}{\ln(z/z_0)} \tag{35b}$$

where u_* denotes the friction wind velocity; $K=0.4$ denotes the Karman constant; z_0 is the surface roughness length, and valued by $z_0=0.05$ m with respect to geomorphic type B.

To simulate the horizontal stochastic wind velocity field, the coordinate system is established setting the direction along the span of the bridge as *x*-axis. Specifically, the left endpoint of the span direction is set as the origin, i.e., $x=0$ m, thus the coordinate of the right endpoint is $x=1000\mathrm{m}$. In this study, three positions of coordinates $x_1=125\mathrm{m}$, $x_2=150\mathrm{m}$ and $x_3=200\mathrm{m}$, i.e., the 1001th, 1201th and 1601th point in the DR-FWSR-I, are selected as the simulated points to generate the representative samples of the stochastic wind velocity fields as a typical study. In addition, with the intention of quantitatively evaluating the simulation accuracy and efficiency of the proposed methods, four evaluation indexes (Liu *et al*. 2017) are employed in this study, including the mean error, the standard deviation error and the auto PSD error of the simulated wind velocity filed, as well as the expense in computational time. Especially, for reflecting the effect of actual PSD values on error, the weighted auto PSD error can be defined as follows

$$\varepsilon_{\mathrm{PSD}}=\sum_{i=1}^{N}\frac{|\,\hat{S}_0(\omega_i)-S_0(\omega_i)\,|}{S(\omega)}\times 100\% \tag{36a}$$

$$S(\omega)=\sum_{i=1}^{N}S_0(\omega_i) \tag{36b}$$

where $\hat{S}_0(\omega_i)$ denotes the estimated auto PSD function at the *i*-th frequency point; $S_0(\omega_i)$ denotes the corresponding target auto PSD function at the *i*-th frequency point; $S(\omega)$ denotes the sum of auto PSD function of the stochastic field.

Meanwhile, the comparisons with the conventional Monte Carlo methods upon the four cases of n_{sel} (the number of representative samples) is 233, 377, 610 and 987 are proceeded to further demonstrate the superiority and effectiveness of the proposed methods. Corresponding to the three proposed dimension-reduction methods, the three Monte Carlo methods are named as MC-CPOD, MC-FWSR-I and MC-FWSR-II, respectively.

The average-relative-error (ARE) for every simulated point refers to Eq. (36) and the reference (Liu *et al*. 2017). The mean values of the average-relative-errors (M-AREs) for the above three positions upon the mean, standard deviation and auto PSD with respect to both the proposed methods and the Monte Carlo methods are calculated for comparison purposes, shown in Fig. 1. It can be seen that all the M-AREs decrease as the number of the sample functions increase, indicating the proposed method has a good robustness. For the M-AREs upon the mean, the proposed schemes all have a better accuracy than the conventional Monte Carlo schemes, while for the M-AREs upon the standard deviation and the auto PSD, the accuracy does not vary obviously. In addition, the CPODs, DR-CPOD and MC-CPOD included, totally behave better than the FWSR-Is, DR-FWSR-Is and MC-FWSR-Is included, in the standard deviation and auto PSD error, which indicates the superiority of the CPODs. Moreover, as clearly presented in the figures, except the M-AREs upon the mean, FWSR-IIs, DR-FWSE-II and MC-FWSR-II included, possess lower M-AREs for both the standard deviation and the auto PSD than the FWSR-Is, which fully reveal the superiority of the proposed scheme using the non-uniform

Table 1 Parameter values of the horizontal stochastic wind velocity field

Parameters	Values	Parameters	Values
Length of the main span (m)	$L = 1000$	Duration (s)	$T = 1024$
Height of the deck above ground (m)	$z = 30$	Geomorphic type	B
Average wind velocity on deck (m/s)	$\bar{u}_z = 34$	Number of the eigenvalue terms	$M_1 = 500$
Number of the wavenumber terms	$M_2 = 4096$	Number of the frequency terms	$N = 2048$
Space interval (m)	$\Delta x = 0.125$	Time interval (s)	$\Delta t = 0.25$
Wavenumber interval (rad/m)	$\Delta\kappa = 0.00613$	Frequency interval (rad/s)	$\Delta\omega = 0.00613$
Number of the wavenumber terms	$M_3 = 3072$	$M_3^{(1)} = 2048$	$M_3^{(2)} = 1024$
Wavenumber interval (rad/m)	$\Delta\kappa_1 = 0.00153$	Space interval (m)	$\Delta x_1 = 1$
Wavenumber interval (rad/m)	$\Delta\kappa_2 = 0.0245$	Space interval (m)	$\Delta x_2 = 0.125$

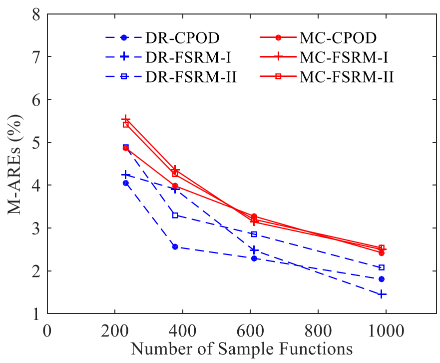

(a) M-AREs of the mean

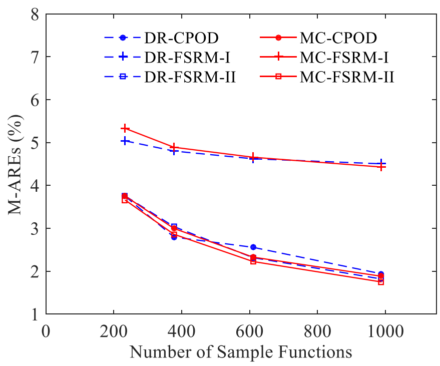

(b) M-AREs of the standard deviation

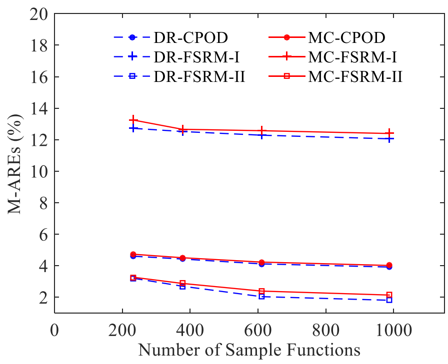

(c) M-AREs of the auto PSD

Fig. 1 Accuracy comparisons between the proposed methods and the conventional Monte Carlo methods

wavenumber intervals for the FWSR. Thus, the effectiveness of the proposed methods is exposed remarkably. At this point, since the accuracy is acceptable when the n_{sel} is around 300, the following will take the case of $n_{sel} = 377$ as examples for illustrative purposes.

Fig. 2 shows the representative samples of the horizontal stochastic wind velocity field at the above three positions in case of $n_{sel} = 377$ generated by the three proposed dimension-reduction approaches, respectively. It can be clearly seen that the time-history curves have the typical characteristics of the fluctuating wind velocity, which indicates that the simulated stochastic wind velocity field is a zero-mean stationary stochastic field.

Figs. 3 and 4 show the comparisons upon the mean and standard deviation (Std.D) between the simulated values by the proposed methods and the corresponding target ones. Evidently, the simulated values fit the target quiet well

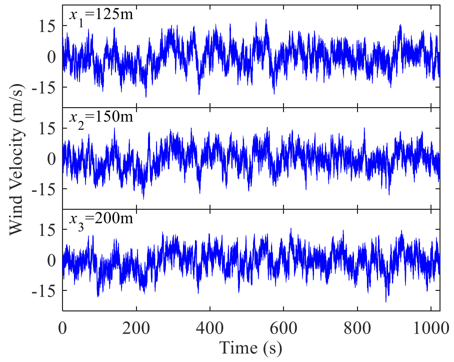

(a) Representative samples of the fluctuating wind velocity by DR-CPOD

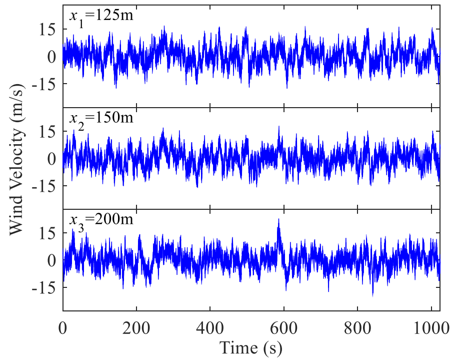

(b) Representative samples of the fluctuating wind velocity by DR-FWSR-I

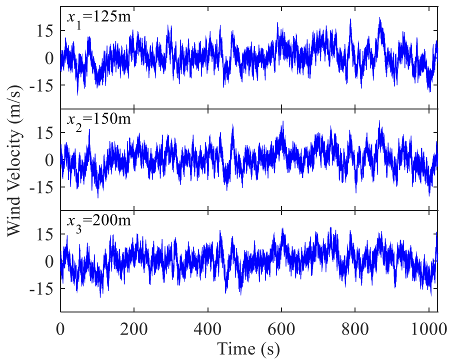

(c) Representative samples of the fluctuating wind velocity by DR-FWSR-II

Fig. 2 Representative samples of the stochastic wind velocity field generated by the proposed methods in case of $n_{\mathrm{sel}} = 377$

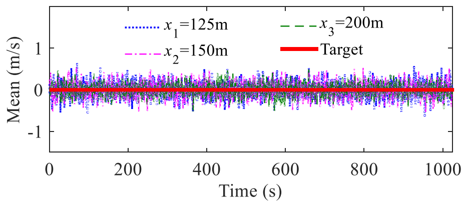

(a) Comparison upon the mean between simulated values and target value by DR-CPOD

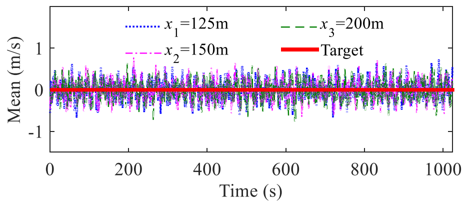

(b) Comparison upon the mean between simulated values and target value by DR-FWSR-I

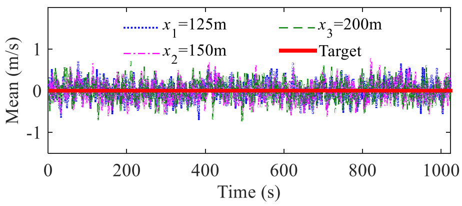

(c) Comparison upon the mean between simulated values and target value by DR-FWSR-II

Fig. 3 Comparison upon the mean between simulated values and target values in case of $n_{\mathrm{sel}} = 377$

except the standard deviation of the DR-FWSR-I is slightly off the target, which is also reflected in Fig. 1(b) and again validates the superiority of the improved scheme adopting the non-uniform wavenumber intervals.

Figs. 5 and 6 present the results of comparisons upon the auto/cross PSD function between the simulated values and the corresponding target values, respectively. By inspection of the figures, one can see that the estimated PSD curves generated by the DR-CPOD seem to be consistent well with the target curves in the low frequency component, while a certain deviation occurs in the high frequency component. Conversely, the estimated PSD curves by the FWSR-Is

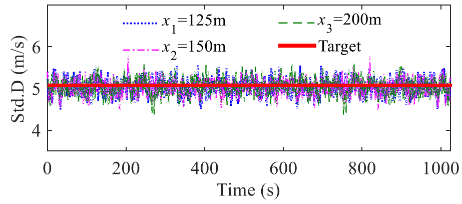

(a) Comparison upon the standard deviation of simulated values with target value by DR-CPOD

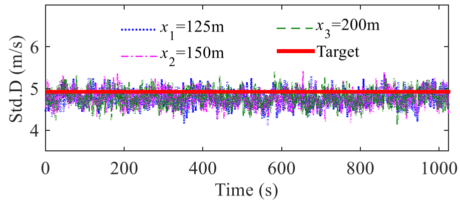

(b) Comparison upon the standard deviation of simulated values with target value by DR-FWSR-I

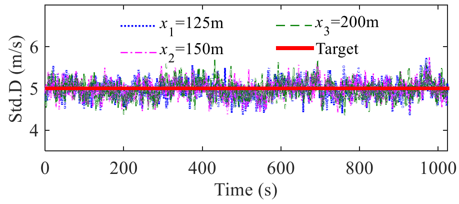

(c) Comparison upon the standard deviation of simulated values with target value by DR-FWSR-II

Fig. 4 Comparison upon the standard deviation between simulated values and target values in case of $n_{\mathrm{sel}} = 377$

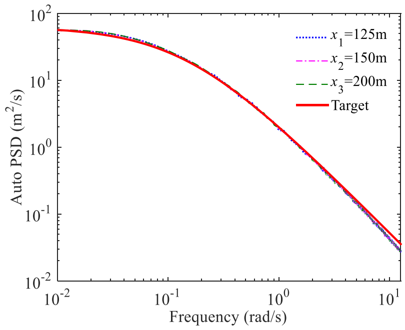

(a) Comparison upon the auto PSD of simulated values with target value by DR-CPOD

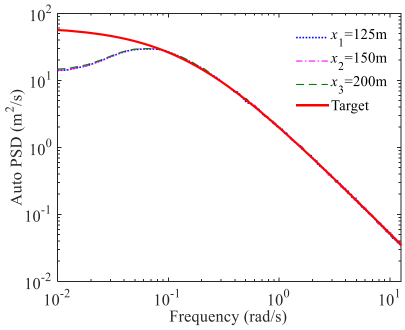

(b) Comparison upon the auto PSD of simulated values with target value by DR-FWSR-I

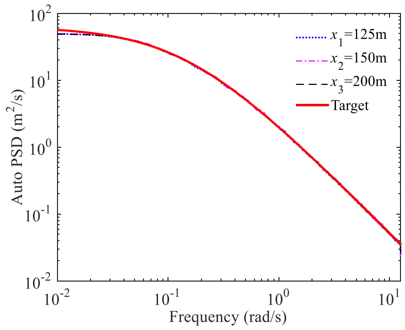

(c) Comparison upon the auto PSD of simulated values with target value by DR-FWSR-II

Fig. 5 Comparison upon the auto PSD between simulated values and target values in case of $n_{\mathrm{sel}} = 377$

coincide perfectly well with the target curves in almost the whole frequency domain except a few frequency points possessing high power in the low frequency component, which results in relatively big M-AREs upon the PSD as shown in Fig. 1(c). It is owing to that the actual value of PSD has been taken into consideration of the M-AREs upon PSD. Fortunately, since the FWSR-IIs can successfully combine the advantages of the above two methods, it thus has a remarkable precision upon PSD in both the low and high frequency component, which strongly validates the effectiveness of the improved scheme.

Fig. 7 shows the comparison of the simulation efficiency with respect to the proposed methods and the conventional Monte Carlo methods. As shown in the figure, it is obvious that the computation time of the CPODs is much less than that of the FWSR-Is and FWSR-IIs. Moreover, the proposed schemes, say the FWSR-IIs employing the non-uniform wavenumber intervals, own a dramatically improvement in the simulation efficiency compared with the FWSR-Is. However, as afore-mentioned, the employment of FFT algorithm regarding the wavenumber would result in a significant saving in the average computation time for each sample generation of numerous spatial points by means of the FWSR-Is or FWSR-IIs, even the average computation time is less than that taken by the CPODs. In addition, though the conventional Monte Carlo methods seem to offer a higher efficiency, in fact, only several seconds are required to generate a representative sample and only a few hundred representative samples are needed to obtain a satisfactory accuracy using the dimension-reduction methods. Thus, the difference in simulation efficiency can be completely ignored in practical applications for structural dynamic response analysis. As a result, the simulation efficiency of the proposed methods can be considered acceptable through the above investigations.

From the above analysis, the following two remarks can be summarized.

i) The above three representations all have their own features. Specifically, the CPODs have superiority in simulation efficiency for sample generation involving a small number of simulated points, and the error upon the

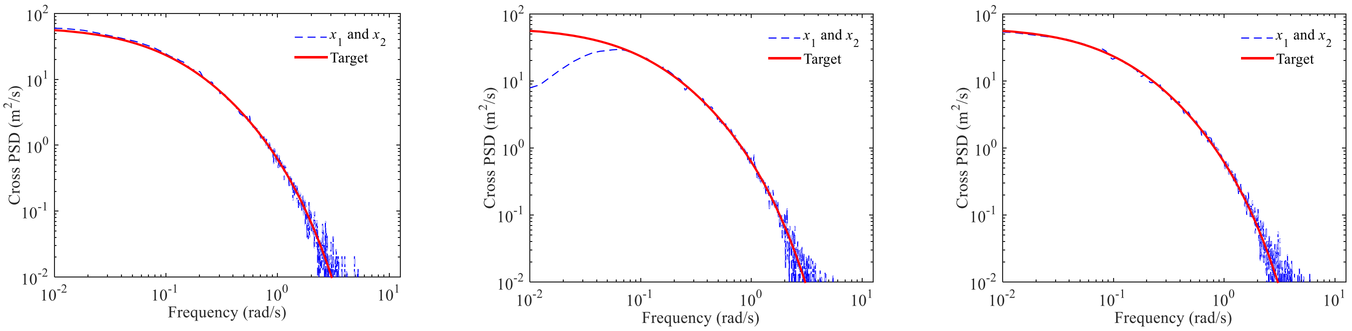

(a) Comparison upon the cross PSD of simulated values with target value by DR-CPOD

(b) Comparison upon the cross PSD of simulated values with target value by DR-FWSR-I

(c) Comparison upon the cross PSD of simulated values with target value by DR-FWSR-II

Fig. 6 Comparison upon the cross PSD between simulated values and target values for x_1 and x_2 in case of $n_{\text{sel}} = 377$

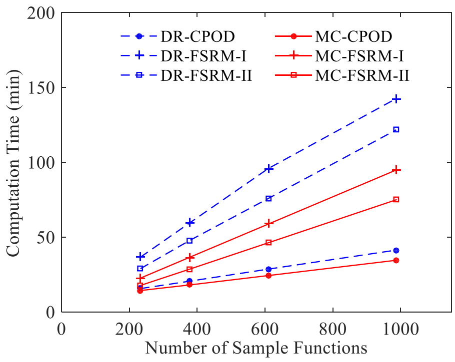

Fig. 7 Comparison upon the calculation time between the proposed methods and the Monte Carlo methods

PSD mainly concentrated in the high frequency component. In contrast, as for the FWSR-Is, the accuracy upon the PSD in the low frequency component should be considered more seriously. In spite of the above, the FWSR-IIs, characterized by the connection of the merits involved in the above two representations, possess a prominent improvement in both the simulation accuracy and efficiency for the FWSR, which makes it can be more extensively applied in numerical simulation of stochastic fields.

ii) Compared with the conventional Monte Carlo methods, the proposed dimension-reduction methods offer more satisfactory results in simulation accuracy. Furthermore, in practical dynamic response analysis of complex randomly-excited structures, just several hundred representative samples are required in the proposed dimension-reduction methods to instead of tens of thousands of sample functions involved in the conventional Monte Carlo methods to achieve the same acceptable simulation accuracy. Consequently, though the simulation efficiency of the proposed methods is relatively inferior compared with the Monte Carlo schemes, it can still be concluded that the proposed methods have a higher simulation efficiency by comprehensively considering the calculation time required for structural dynamic response analysis.

6. Conclusions

This study deduces the original spectral representations based on the CPOD and the FWSR of the stationary stochastic fields, and the relations between the two are detailedly discussed. Then the dimension-reduction methods are proposed to simulate the stochastic wind velocity fields using merely one elementary random variable. In addition, the improved scheme adopting non-uniform wavenumber intervals is suggested to effectively enhance the accuracy of standard deviation and PSD function in the low frequency component and simulation efficiency for the FWSR. Finally, numerical examples elaborate the peculiar features of the three representations, say the CPODs, the FWSR-Is and the FWSR-IIs. The validity and effectiveness of the proposed dimension-reduction methods are also adequately demonstrated through comparison with the conventional Monte Carlo methods. The main characteristics of the proposed dimension-reduction methods drawn from this study can be summarized as follows.

i) The dimension-reduction methods can effectively reduce the high dimension of random variables to merely one. Generally, millions of random variables are required in the conventional Monte Carlo methods; however, the extremely low dimension of the random variable involved in the proposed methods can successfully bypass the difficulties suffered from the conventional Monte Carlo methods. Besides, the dimension-reduction methods can be further integrated with FFT algorithm to significantly improve the simulation efficiency.

ii) The simulation accuracy and efficiency of the FWSR can be greatly improved simultaneously through adopting the non-uniform wavenumber intervals. Correspondingly, it is believed that the simulation accuracy and efficiency can also be enhanced by introducing the non-uniform frequency intervals. In fact, this scheme can also be applied to the CPOD, even the SRM and the POD.

iii) The probability information of the representative samples generated by the proposed dimension-reduction methods is well reflected. Since the dimension-reduction methods are achieved by just one elementary random variable with the representative points set, each representative sample of the fluctuating wind velocity fields is generated with an assigned probability, and all the probabilities of the representative samples can ensemble a complete probability set. Therefore, it proves a solid foundation for the proposed dimension-reduction methods being combined with the PDEM to accurately analyze the dynamic response and evaluate dynamic reliability of complex wind-induced structures in engineering practices.

Acknowledgements

This work was supported by the National Natural Science Foundation of China (Grant Nos. 51978543, 51778343 and 51278282). These financial supports are gratefully acknowledged. Ph.D. Candidate Zixin Liu is greatly appreciated for her constructive discussion and comment on the research.

References

Benowitz, B.A. and Deodatis, G. (2015), "Simulation of wind velocities on long span structures: a novel stochastic wave based model". *J. Wind Eng. Ind. Aerod.*, **147**, 154-163. https://doi.org/10.1016/j.jweia.2015.10.004.

Carassale, L. and Solari, G. (2002), "Wind modes for structural dynamics: a continuous approach", *Probabilist. Eng. Mech.*, **17**(2), 157-166. https://doi.org/10.1016/s0266-8920(01)00036-4.

Chen, J.B., He, J.R., Ren, X.D. and Li, J. (2018), "Stochastic harmonic function representation of random fields for material properties of structures", *J. Eng. Mech.*, **144**(7), 04018049. https://doi.org/10.1061/(asce)em.1943-7889.0001469.

Chen, J.B., Kong, F. and Peng, Y.B. (2017), "A stochastic harmonic function representation for non-stationary stochastic processes", *Mech. Syst. Signal Pr.*, **96**, 31-44. https://doi.org/10.1016/j.ymssp.2017.03.048.

Chen, J.B., Sun, W.L., Li, J. and Xu, J. (2013), "Stochastic harmonic function representation of stochastic processes", *J. Appl. Mech.*, **80**(1), 011001. https://doi.org/10.1115/1.4006936.

Chen, L.Z. and Letchford, C.W. (2005), "Simulation of multivariate stationary Gaussian stochastic processes: hybrid spectral representation and proper orthogonal decomposition approach", *J. Eng. Mech.*, **131**(8), 801-808. https://doi.org/10.1061/(asce)0733-9399(2005)131:8(801).

Chen, X.Z. and Kareem, A. (2005), "Proper orthogonal decomposition-based modeling, analysis, and simulation of dynamic wind load effects on structures", *J. Eng. Mech.*, **131**(4), 325-339.https://doi.org/10.1061/(asce)0733-9399(2005)131:4(325).

Davenport, A.G. (1961), "The spectrum of horizontal gustiness near the ground in high winds", *Q. J. Roy. Meteor. Soc.*, **87**, 194-211. https://doi.org/10.1002/qj.49708737208.

Deodatis, G. and Shinozuka, M. (1989), "Simulation of seismic ground motion using stochastic waves", *J. Eng. Mech.*, **115**(12), 2723-2737.https://doi.org/10.1061/(asce)0733-9399(1989)115:12(2723).

Di Paola, M. (1998), "Digital simulation of wind field velocity", *J. Wind Eng. Ind. Aerod.*, **74-76**, 91-109. https://doi.org/10.1016/s0167-6105(98)00008-7.

Di Paola, M. and Gullo, I. (2001), "Digital generation of multivariate wind field processes", *Probabilist. Eng. Mech.*, **16**(1), 1-10. https://doi.org/10.1016/s0266-8920(99)00032-6.

Ghanem, R.G. and Spanos, P.D. (1991), "Spectral stochastic finite-element formulation for reliability analysis", *J. Eng. Mech.*, **117**(10), 2351-2372. https://doi.org/10.1061/(asce)0733-9399(1991)117:10(2351).

Glasserman, P. (2013), *Monte Carlo Methods in Financial Engineering*, Springer, New York, NY, USA.

Huang, G.Q. (2015), "Application of proper orthogonal decomposition in fast Fourier transform-assisted multivariate nonstationary process simulation", *J. Eng. Mech.*, **141**(7), 04015015. https://doi.org/10.1061/(asce)em.1943-7889.0000923.

Huang, G.Q., Ji, X.W., Zheng, H.T., Luo, Y., Peng, X.Y. and Yang, Q.S. (2018), "Uncertainty of peak value of non-Gaussian wind load effect: analytical approach", *J. Eng. Mech.*, **144**(2), 04017172. https://doi.org/10.1061/(asce)em.1943-7889.0001402.

Kaimal, J.C., Wyngaard, J.C., Izumi, Y. and Coté, O.R. (1972), "Spectral characteristics of surface-layer turbulence", *Q. J. Roy. Meteor. Soc.*, **98**, 563-589. https://doi.org/10.1256/smsqj.41706.

Kanwal, P. (1971), *Linear Interval Equations*, Academic Press, New York, NY, USA.

Khanduri, A.C., Stathopoulos, T. and Bédard, C. (1998), "Wind-induced interference effects on buildings — a review of the state-of-the-art", *Eng. Struct.*, **20**(7), 617-630. https://doi.org/10.1016/s0141-0296(97)00066-7.

Li, J. and Chen, J.B. (2009), *Stochastic Dynamics of Structures*, John Wiley & Sons, Singapore.

Liu, Z.H., Liu, Z.J., He, C.G. and Lu, H.L. (2019), "Dimension-reduced probabilistic approach of 3-D wind field for wind-induced response analysis of transmission tower", *J. Wind Eng. Ind. Aerod.*, **190**, 309-321. https://doi.org/10.1016/j.jweia.2019.05.013.

Liu, Z.J. and Liu, Z.H. (2018), "Random function representation of stationary stochastic vector processes for probability density evolution analysis of wind-induced structures", *Mech. Syst. Signal Pr.*, **106**, 511-525. https://doi.org/10.1016/j.ymssp.2018.01.011.

Liu, Z.J., Liu, W. and Peng, Y.B. (2016), "Random function based spectral representation of stationary and non-stationary stochastic processes", *Probabilist. Eng. Mech.*, **45**, 115-126. https://doi.org/10.1016/j.probengmech.2016.04.004.

Liu, Z.J., Liu, Z.H. and Peng, Y.B. (2018a), "Simulation of multivariate stationary stochastic processes using dimension-reduction representation methods", *J. Sound Vib.*, **418**, 144-162. https://doi.org/10.1016/j.jsv.2017.12.029.

Liu, Z.J., Liu, Z.X. and Chen, D.H. (2018b), "Probability density evolution of a nonlinear concrete gravity dam subjected to nonstationary seismic ground motion", *J. Eng. Mech.*, **144**(1), 04017157. https://doi.org/10.1061/(asce)em.1943-7889.0001388.

Liu, Z.J., Liu, Z.X. and Peng, Y.B. (2017), "Dimension reduction of Karhunen-Loeve expansion for simulation of stochastic processes", *J. Sound Vib.*, **408**, 168-189. https://doi.org/10.1016/j.jsv. 2017.07.016.

Peng, L.L., Huang, G.Q., Kareem, A. and Li, Y.L. (2016), "An efficient space–time based simulation approach of wind velocity field with embedded conditional interpolation for unevenly spaced locations", *Probabilist. Eng. Mech.*, **43**, 156-168. https://doi.org/10.1016/j.probengmech.2015.10.006.

Peng, Y.B., Wang, S.F. and Li, J. (2018), "Field measurement and investigation of spatial coherence for near-surface strong winds in Southeast China", *J. Wind Eng. Ind. Aerod.*, **172**, 423-440. https://doi.org/10.1016/j.jweia.2017.11.012.

Priestley, M.B. (1965), "Evolutionary spectra and non-stationary processes", *J. R. Stat. Soc. B*, **27**(2), 204-237. https://doi.org/10.1111/j.2517-6161.1965.tb01488.x.

Shinozuka, M. (1971), "Simulation of multivariate and multidimensional random processes", *J. Acoust. Soc. Am.*, **49**(1), 357-368. https://doi.org/10.1121/1.1912338.

Shinozuka, M. and Deodatis, G. (1996), “Simulation of multi-dimensional Gaussian stochastic fields by spectral representation”, *Appl. Mech. Rev.*, **49**(1), 29-53. https://doi.org/10.1115/1.3101883.

Shinozuka, M. and Jan, C.M. (1972), “Digital simulation of random processes and its applications”, *J. Sound Vib.*, **25**(1), 111-128. https://doi.org/10.1016/0022-460X(72)90600-1.

Solari, G. and Carassale, L. (2001), “Model transformation tools in structural dynamics and wind engineering”, *Wind Struct.*, **3**(4), 221-241. https://doi.org/10.12989/was.2000.3.4.221.

Song, Y.P., Chen, J.B., Peng, Y.B., Spanos, P.D. and Li, J. (2018), “Simulation of nonhomogeneous fluctuating wind speed field in two-spatial dimensions via an evolutionary wavenumber-frequency joint power spectrum”, *J. Wind Eng. Ind. Aerod.*, **179**, 250-259. https://doi.org/10.1016/j.jweia. 2018.06.005.

Wu, Y.X., Gao, Y.F., Li, D.Y., Xu, C.J. and Mahfouz A.H. (2013), “Approximation approach to the SRM based on root decomposition in the simulation of spatially varying ground motions”. *Earthq. Eng. Eng. Vib.*, **12**(3), 363-372. https://doi.org/10.1007/s11803-013-0178-9.

Wu, Y.X., Gao, Y.F., Zhang, N. and Zhang, F. (2018), “Simulation of spatially varying non-Gaussian and nonstationary seismic ground motions by the spectral representation method”, *J. Eng. Mech.*, **144**(1), 04017143. https://doi.org/10.1061/(asce)em. 1943-7889.0001371.

Yang, J.N. (1972), “Simulation of random envelope processes”, *J. Sound Vib.*, **21**(1), 73-85. https://doi.org/10.1016/0022-460x (72)90207-6.

Zerva, A. (1992), “Seismic ground motion simulations from a class of spatial variability models”, *Earthq. Eng. Struct. D.*, **21**(4), 351-361. https://doi.org/10.1002/eqe.4290210406.

Zhu, S.Y., Li, Y.L., Togbenou, K., Yu, C.J. and Xiang, T.Y. (2018), “Case study of random vibration analysis of train-bridge systems subjected to wind loads”, *Wind Struct.*, **27**(6), 399-416. https://doi.org/10.12989/was.2018.27.6.399.

Zu, G.B. and Lam, K.M. (2018), “Across-wind excitation mechanism for interference of twin tall buildings in tandem arrangement”, *J. Wind Eng. Ind. Aerod.*, **177**, 167-185. https://doi.org/10.1016/j.jweia.2018.04.019.

FR